Pharm Res (2012) 29:1143–1157
DOI 10.1007/s11095-012-0698-4

RESEARCH PAPER

Dehydration Kinetics and Crystal Water Dynamics of Carbamazepine Dihydrate

K. Kachrimanis • U. J. Griesser

Received: 16 November 2011 / Accepted: 27 January 2012 / Published online: 8 February 2012

ABSTRACT

Purpose To investigate the dehydration of carbamazepine dihydrate, combining kinetics and crystal water dynamics with electronic structure calculations.

Methods Thermal microscopy, moisture sorption, and thermogravimetric analysis (TGA) were applied to evaluate the effects on relative humidity (RH) and temperature, while crystal water dynamics were monitored by 2D-FTIR correlation spectroscopy (2DCOS) and the nature of the H-bonding network was investigated by 3D-periodic DFT calculations.

Results It was found that the dihydrate is unstable below 40% RH and/or above the glass transition temperature (T_g~53°C). At room temperature, amorphous carbamazepine is formed at RH~0%, form I at RH~10%, and mixtures of forms I and III at higher RH. Above the T_g, the dehydration yields partially crystalline mixtures of forms I and IV between 50–100°C, and form I above 100°C. In all cases, the amorphous product crystallizes to form IV. Thermal analysis and 2DCOS revealed a biphasic dehydration process. Kinetic modelling suggests a diffusion-controlled dehydration below T_g *and reaction interface-controlled kinetics above* T_g.

Conclusions The dehydration consists of two overlapping water removal processes, with the water molecule attached to the amide C=O departing faster, probably due to the destabilizing effect of anti-bonding interactions between the water H1s and the carbonyl O2p orbital.

K. Kachrimanis (✉)
Department of Pharmaceutical Technology, School of Pharmacy
University of Thessaloniki
54124 Thessaloniki, Greece
e-mail: kgk@pharm.auth.gr

U. J. Griesser
Department of Pharmaceutical Technology, Institute of Pharmacy
Innsbruck University
Innrain 52
6020 Innsbruck, Austria

KEY WORDS 2d correlation spectroscopy · carbamazepine dihydrate · dehydration kinetics · DFT calculations

INTRODUCTION

Hydrate formation is a common problem that may occur during manufacturing processes where water is brought into contact with the active pharmaceutical ingredients and excipients, or upon exposure of the raw materials and/or finished products to environmental humidity (1). Crystal hydrates may differ substantially to the anhydrate forms in regard to critical properties such as solubility and dissolution rate, sometimes leading to bioavailability problems. Removal of water molecules from the crystal lattice (dehydration) is often induced during manufacturing processes that involve the application of thermal or mechanical stress (e.g. drying, milling, mixing, tablet compaction), however in most cases it is not possible to predict the solid form of the dehydration product (2). A unified model for the classification of dehydration reactions based on the structural filiation between the mother phase and the resultant product has been suggested by Petit and Coquerel (3), while a classification scheme for the dehydrations "water evolution type" of molecular crystals that is based on the physical state of reaction products has been proposed by Galwey (4). Depending on the dehydration conditions and structural and energetic aspects, the substance may retain crystallinity, or the lattice may collapse into an amorphous product, which is likely to crystallize to a metastable polymorph according to Ostwald's rule of stages. Therefore, the study of dehydration reactions is important from a practical, as well as a theoretical viewpoint, since it provides information useful for the prediction of the hydrate's stability range and selection of optimal dehydration protocols, while understanding of the dehydration mechanism can provide insights into the bonding structure and energetics of the lattice. A convenient approach to the study of dehydration reactions is the

selection of a well characterized model substance capable of forming hydrates and monitoring the course of the dehydration by a suitable experimental technique, such as thermogravimetric analysis (TGA) or vibrational spectroscopy methods (FTIR, FT-Raman etc.) (5,6). Several polymorphic substances have been used as model drugs for the study of hydration-dehydration reactions, such as theophylline (7), piroxicam (8), or carbamazepine (9). However, most dehydration studies deduce the reaction mechanism on the basis mainly of kinetic data, rarely taking into consideration the dynamics of crystal water at the molecular level (10).

In the present work, an integrated approach is applied to the investigation of crystal dehydration, which combines reaction kinetics and crystal water dynamics data with electronic structure calculations. The dihydrate of carbamazepine is selected as a model substance, since carbamazepine is a well characterized active pharmaceutical ingredient capable of showing crystal polymorphism and related phenomena. It is known to exist in four anhydrous forms (11), a dihydrate (12), as well as numerous solvates and molecular adducts (13). The presence of carbamazepine dihydrate in commercial tablet formulations of the pharmaceutically preferred form III is considered as the major cause of bioavailability problems that has even led to a recall of products from the market (14) because of its very low solubility (15). The structure of the dihydrate was finally proven to be monoclinic (space group $P2_1/c$, unit cell dimensions: a= 10.066, b=28.719, c=4.831 Å, β=103.45°) exhibiting multiple micro-twinning that emulates orthorhombic symmetry (16–18), in contrast to the initially reported as orthorhombic with rotational disorder of the amide group (12,19).

Investigations of the dehydration of carbamazepine dihydrate have shown that the resulting anhydrous form can be amorphous or crystalline depending on the temperature and environmental humidity (20,21). However, the mechanism of dehydration has not been fully clarified, as the numerous studies that have been performed in the past, resulted in conflicting reports regarding the dehydration products (amorphous *versus* crystalline form IV, III or I) and the corresponding dehydration conditions (relative humidity and temperature) favouring their formation (9,22–24). Furthermore, the possibility of existence of different dihydrates (25), as well as of the formation of a partly (de)hydrated intermediate (22) has been suggested, while the dehydration has been characterized as a two-step process (26). Additionally, different dehydration kinetics and corresponding activation energies have been reported for similarly prepared samples (9,22).

Therefore, the effects of environmental relative humidity (RH) and temperature on the dehydration mechanism and the resulting anhydrous form are investigated by optical and thermal microscopy observations, kinetic analysis of gravimetric moisture sorption and isothermal thermogravimetric analysis (TGA) data, evaluation of crystal water dynamics by generalized 2D FTIR correlation spectroscopy (2DCOS), while the nature of hydrogen bonding interactions between carbamazepine and crystal water are modelled using quantum mechanical 3D periodic DFT calculations.

MATERIALS AND METHODS

Materials

Carbamazepine (P-monoclinic, form III), purchased by Pfannenschmidt (D-Hamburg, Germany), was used as a starting material.

Absolute ethanol, purchased by Merck (Darmstadt, Germany), was used in mixtures with distilled water as the crystallization solvent.

Phosphorous pentoxide, potassium hydroxide, potassium acetate, magnesium chloride, potassium carbonate, potassium thiocyanate, sodium bromide, sodium chloride, potassium chloride, zinc sulphate, and potassium sulphate of analytical grade, all purchased from Merck (Darmstadt, Germany) were used for the preparation of saturated solutions to generate atmosphere of 0%, 9%, 23%, 30%, 43%, 46%, 61%, 75%, 84%, 92%, and 98% relative humidity, respectively.

Methods

Crystallization of Carbamazepine Dihydrate

Two batches of carbamazepine dihydrate crystals were produced by dissolving 15 g of carbamazepine in 400 ml of a boiling water-ethanol mixture (3:1 *w*/*w*). The clear solution was left to slowly cool down at ambient temperature in a water bath for 14 h and prismatic crystals of length 250–1000 μm and width 25–150 μm were harvested by filtration. In order to obtain a smaller particle size batch, the process was repeated applying lower cooling temperature (~5°C) and intense agitation. The crystals obtained this way had a length between 20 and 300 μm and width 2–30 μm. The samples were subsequently stored in closed desiccators above NaCl solutions at 75% RH.

Optical Microscopy

Orthoscopic and conoscopic observation of carbamazepine dihydrate crystals was performed on a PriorluxPol petrological microscope (Prior, UK) equipped with a quarter wave retardation plate for the determination of the optical sign of the crystals.

For the observation of the dehydration in dry atmosphere, a VGI2000M accessory (Surface Measurement

Systems Inc, London, UK) was attached to the microscope and the sample was conditioned at 0% RH and 25°C.

For thermomicroscopic investigations the microscope was equipped with a Kofler hot stage (Reichert Thermovar, Vienna, Austria). Photomicrographs were acquired using an Olympus DP50 microscope stage digital camera with a resolution of 5.8 million pixels, operated through the AnalySIS 3.2 software (Soft Imaging System GmbH, Hamburg, Germany).

Crystal Morphology Modelling

The morphology of carbamazepine dihydrate crystals was modelled within the framework of the attachment energy theory, using the crystal structure of (8) (CSD ref code FEFNOT02) as a starting geometry. The attachment energy is defined as the energy per molecule that is released when a new layer is attached to the surface of the crystal, and therefore provides a measure of the thermodynamic stability of each crystal face. Consequently, those faces with the more exothermic attachment energy will tend to grow faster and become morphologically less important. The morphology calculated this way is commonly called "growth" morphology because it reflects crystal growth under kinetic control.

The GDIS program (27) was used to construct a preliminary morphology model based on Bravais-Friedel-Donnay-Harker (BFDH) theory (which assumes that the slowest growing faces are those with the greatest interplanar spacing, d_{hkl}) in order to identify those faces that are more likely to occur. Subsequently, the energy of those faces was calculated and minimized with the help of the General Utility Lattice Program (GULP v.3.4) (28), using Dreiding 2.21 force field parameters (29) and AM1-BCC atomic point charges (30,31) calculated with the QUACPAC program (OpenEye Scientific Software Inc., USA). Calculated morphologies were visualized on the basis of the Wulff stereographic projection, with the help of GDIS software.

Gravimetric Moisture Desorption

Samples of the large and small particle size batches of the dihydrate were equilibrated at 0%, 9%, 23%, 30%, 43%, 46%, 61%, 75%, 84%, 92%, and 98% relative humidity in closed desiccators above saturated salt solutions for 40 days at 25°C and the equilibrium water content was determined gravimetrically. Subsequently, from the weight change *vs* time data, moisture desorption isotherms were constructed.

Thermogravimetric Analysis and Kinetic Modeling

Accurately weighted (±0.0005 mg) samples of approximately 5 mg were placed into 50 µl platinum pans and subjected to isothermal TGA in the temperature range of 30 to 70°C, using a Perkin-Elmer TGA-7 system (Perkin-Elmer, Norwalk, CT, USA) operated through the Pyris 2.0 software. Crystals of the large particle size batch were also subjected to non-isothermal TGA at heating rates of 0.25, 0.5, 1, 2.5, 5, 10, 15, and 20 K/min in the temperature range from 25 to 200°C, for comparison purposes. Nitrogen was used as purge gas (balance purge: 50 ml/min, sample purge: 25 ml/min).

Kinetic Model Fitting Approach. The kinetics of crystal dehydration can be described by an equation of the general form:

$$\frac{da}{dt} = k(T)f(a) \tag{1}$$

where α represents the dehydrated fraction (ratio between weight loss at time t and the total weight loss at the end of the reaction), k is a temperature-dependent rate constant, and $f(\alpha)$ is the dehydration function whose form depends on the reaction mechanism, and is usually selected from a list of commonly applied models, representative of the most common solid state reaction mechanisms (nucleation and growth, diffusion-controlled, geometric contraction, and reaction order (Table I)). Usually, Eq. 1 is integrated to the form:

$$g(a) = k(T)t \tag{2}$$

where $g(\alpha)$ is the integral form of the kinetic function $f(\alpha)$.

In the present study, the kinetic equations of Table I were fitted to the isothermal TGA data by linear regression, and Arrhenius temperature dependence was assumed for the constant, k (Eq. 2)

$$k(T) = A\exp\left(\frac{-E_\alpha}{RT}\right) \tag{3}$$

where A is the so called pre-exponential factor, E_α is the energy of activation, R is the universal gas constant and T is the temperature. Further, the temperature dependence of constant k was modelled within the framework of transition state theory (32) using the linearized form of the Eyring equation (Eq. 4).

$$\ln\frac{k}{T} = \frac{-\Delta H^{\neq}}{R}\frac{1}{T} + \ln\frac{k_B}{h} + \frac{\Delta S^{\neq}}{R} \tag{4}$$

where k_B is the Boltzmann constant, while $\Delta S^{\neq}$ and $\Delta H^{\neq}$ represent the entropy and enthalpy of the activated complex, respectively. Low $\Delta H^{\neq}$ values (20–150 kJ/mol) correspond to fast rate, while high $\Delta H^{\neq}$ values correspond to slow rate. Large negative $\Delta S^{\neq}$ values indicate an unfavourable reaction, with degrees of freedom being frozen on the way to the transition state, while positive or small negative $\Delta S^{\neq}$ values indicate a favourable reaction (the more disordered the transition state, the faster the reaction).

Table I Kinetic Models Used in the Analysis of Isothermal TGA Dehydration Data

Kinetic model	Differential form $f(a) = \frac{1}{k}\frac{da}{dt}$	Integral form $g(a)=kt$
Reaction order models		
F0 (zero order)	$(1-a)^0$	a
F1 (1st order)	$(1-a)$	$-\ln(1-a)$
F2 (2nd order)	$(1-a)^2$	$(1-a)^{-1}-1$
Nucleation models		
An (JMAK equation)	$n(1-a)[-\ln(1-a)]^{1-1/n}$	$[-\ln(1-a)^{1/n}]$
B1 (prout-Tomkins)	$a(1-a)$	$\ln[a/(1-a)]$
P2 (power law)	$2a^{1/2}$	$a^{1/2}$
P3 (power law)	$3a^{2/3}$	$a^{1/3}$
P4 (power law)	$4a^{3/4}$	$a^{1/4}$
Geometrical contraction models		
R2 (contracting cylinder)	$2(1-a)^{1/2}$	$[1-(1-a)^{1/2}]$
R3 (contracting sphere)	$3(1-a)^{2/3}$	$[1-(1-a)^{1/3}]$
Diffusion models		
D1 (1d diffusion)	$(1/2)a$	a^2
D2 (2d Valensi-Carter)	$[-\ln(1-a)]^{-1}$	$[(1-a)\ln(1-a)]+a$
D3 (3d Jander)	$(3/2)[(1-a)^{2/3}/(1-(1-a)^{1/3})]$	$[1-(1-a)^{1/3}]^2$
D4 (3d Ginstling-Brunshtein)	$(3/2)((1-a)^{-1/3}-1)$	$1-(2/3)a-(1-a)^{2/3}$

Attenuated Total Reflectance (ATR) FTIR Spectroscopy

All ATR-FTIR spectra were acquired using a Shimadzu IR Prestige 21 spectrometer (Shimadzu Europa GmbH, Duisburg, Germany), with a horizontal Golden Gate MkII single-reflection ATR system (Specac, Kent, UK) equipped with a heated diamond top plate, ZnSe lenses and a 4000 series temperature controller. Spectra were recorded sequentially between 4000 and 600 cm^{-1} at a resolution of 4 cm^{-1}. A number of 32 scans were added for each spectrum.

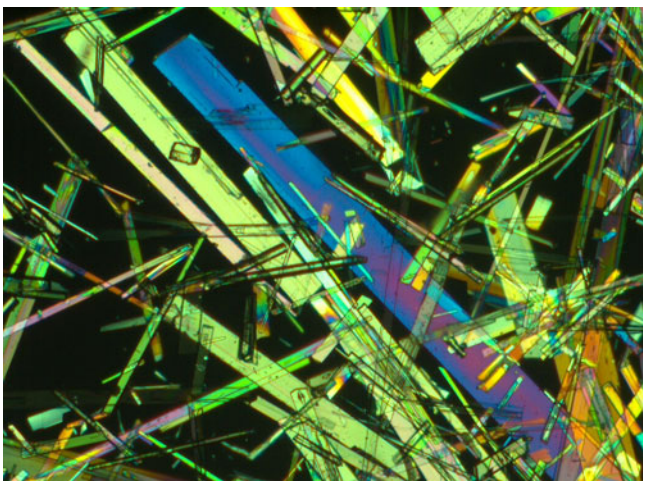

Fig. 1 Carbamazepine dihydrate crystals grown from ethanol/water mixtures, observed under crossed polarisers.

Generalized Two-Dimensional Correlation Spectroscopy. Generalised 2DCOS analysis (33) of the ATR-FTIR spectra was applied in order to monitor the crystal water dynamics during dehydration, since this method is capable not only of probing the vibrations of functional groups, but also of sorting out their corresponding temporal sequence. The spectra were arranged into a matrix and subjected to generalized 2D correlation analysis of the amide C=O (at 1670 cm^{-1}) and N-H stretching vibration (at 3432 cm^{-1} for the dihydrate, 3481 cm^{-1} for form I, and 3470 cm^{-1} for form IV), since these groups are associated with the two crystallographically independent water molecules by hydrogen bonding. Correlation spectra were calculated after subtraction of the mean spectrum from every single spectrum in the matrix (mean-centring), giving the so-called "dynamic" spectra. Subsequently, for the dynamic spectra dataset, y, acquired at m intervals of the perturbation variable t, the synchronous, $\Phi(v_1,v_2)$, and the asynchronous correlation spectrum, $\Psi(v_1,v_2)$, were calculated by:

$$\Phi(\nu_1,\nu_2) = \frac{1}{m-1}\sum_{j=1}^{m}\bar{y}_j(\nu_1).\bar{y}_j(\nu_2)$$

and

$$\Psi(\nu_1,\nu_2) = \frac{1}{m-1}\sum_{j=1}^{m}\bar{y}_j(\nu_1).\sum_{k=1}^{m}N_{jk}\bar{y}_k(\nu_2)$$

where $\bar{y}(\nu_1,t)$ is the intensity of the dynamic spectrum at wavelength v_1, $\bar{y}(\nu_2,t)$ the intensity of the dynamic spectrum

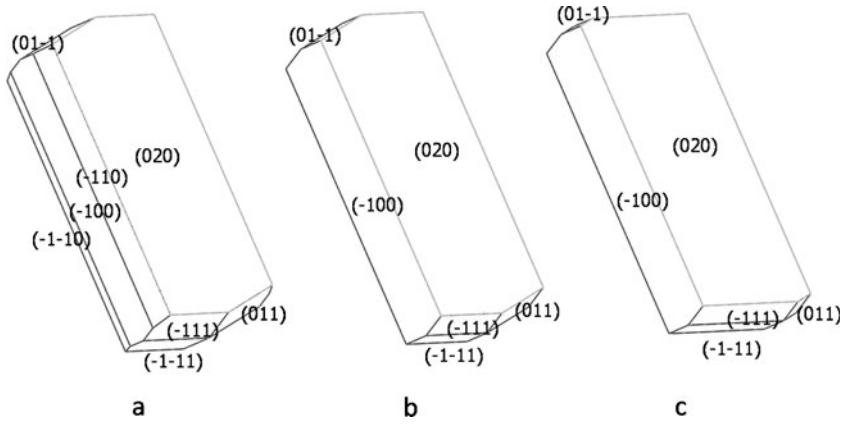

Fig. 2 Computational morphology models according to BFDH (**a**) and Attachment Energy theory before (**b**) and after surface relaxation (**c**).

at wavelength v_2, and N_{jk} are the Hilbert transformation matrix elements, given by:

$$N_{jk} = \begin{cases} 0, & j = k \\ \frac{1}{\pi(k-j)}, & otherwise \end{cases}$$

The synchronous correlation intensity represents the concomitant changes between the two spectra, while the asynchronous correlation represents the out-of-phase changes. The sign of the synchronous peaks shows whether the two spectra change in the same (positive) or in opposite directions (negative), while the sign of the peaks of the asynchronous 2D correlation spectrum reveals the relative temporal relationship or order of events in the submolecular motions taking place during the reaction studied. According to the so-called Noda's rules (33), if the signs of synchronous and asynchronous peaks are the same, then the signal intensity variation at the X axis (x_1) occurs predominantly before (or faster than) that at the Y axis (x_2). If the signs are different, then x_1 changes predominantly after (or slower than) x_2. If there is no asynchronous correlation peak, then the changes are considered to occur simultaneously, while if there is no synchronous correlation peak, the temporal relationship of the changes cannot be determined.

Synchronous and asynchronous 2D correlation spectra were calculated using the 2Dshige software program (Shigeaki Morita, Kwansei-Gakuin University).

Table II Unrelaxed and Relaxed Attachment Energies of the Morphologically Important Crystal Faces, Calculated in Vacuum

Miller index	Attachment Energy (eV.mol^{-1})		% change
(hkl)	unrelaxed	relaxed	
(020)	−0.2099	−0.2202	4.9
(100)	−0.1399	−0.1433	2.4
(1–10)	−0.1731	−0.3691	3.4
(11–1)	−0.3698	−0.3691	−0.2
(01–1)	−0.4046	−0.4127	2.0

Electronic Structure Calculations

The electronic structure of carbamazepine dihydrate was modeled on the basis of periodic DFT calculations within the local density approximation (LDA). Norm-conserving pseudopotentials developed according to the Troullier and Martins scheme (34), and DZP numerical atomic basis orbitals were used for the description of valence electrons. An exchange-correlation function parametrized using an empirical correction to account for Van der Waals interactions (35), was used for the calculation of electron density, and the numerical integrals were evaluated in a real space grid defined by cut-off energy of 200 Ry. A Monkhorst-Pack 4×4×4 k grid was used to sample the Brillouin zone. Geometry optimization was carried out by the Conjugate Gradient algorithm for the position of all 144 atoms in the unit cell keeping its volume fixed, until the SCF energy was converged to 1×10^{-4} Ry. Based on the optimized structure, the crystal orbital Hamilton population, COHP (36), of the crystal water and amide group atoms involved in hydrogen bonding was evaluated. Negative peaks in the COHP plots indicate that the interaction leads to a lower energy state (bonding), while positive peaks indicate an increase in energy (anti-bonding interaction).

The Siesta code (37) was used for the periodic DFT calculations (available from: http://www.icmab.es/siesta/).

RESULTS AND DISCUSSION

Crystal Morphology

A characteristic photomicrograph of carbamazepine dihydrate crystals grown from ethanol/water mixtures, taken under crossed polarizers, is shown in Fig. 1. The crystals are strongly birefringent and exhibit an elongated, "bladed" habit. When the crystals are observed under crossed polarizers and a quarter wave retardation plate is inserted with its slow axis perpendicular to the crystal elongation axis, birefringence goes up the

Table III Decomposition of the Total Lattice Energy of the Optimized Structure Non-Bonded, Bonded, and Electrostatic Components

Energy component	Energy ($eV.mol^{-1}$ unit cells)
Non-bonded (Van der Waals)	5.810
Three-body potentials	1.331
Four-body potentials	7.435
Electrostatic (Coulomb)	−21.289
Total	−6.713

scale of the Michele Levy chart (first order sky-blue turns first order green), while when it is inserted with its slow axis parallel to the crystal elongation axis, birefringence goes down (first order sky-blue turns to first order orange-red), indicating that the optic sign of the crystal is negative (length-slow).

Computational morphology models (Fig. 2) calculated according to BFDH (Fig. 2a), and Attachment Energy (AE) theory before (Fig. 2b) and after surface relaxation (Fig. 2c), are in good agreement with the experimental morphology, confirming the suitability of Dreiding 2.21 force field parameters in combination with AM1 BCC atomic charges for the calculation. All models correctly predict that the (020) face is the slowest growing face and thus the morphologically most important one. The effect of surface relaxation, although it does not result in energy changes larger than 5% (Table II) was found to be significant on the resultant calculated morphology, as it increases the similarity between the predicted and experimental morphology. Furthermore, the crystal lattice energy decomposition (Table III) reveals that the electrostatic component has a strong negative relative contribution, which is more significant than the Van der Waals non bonded interactions, outlining the great importance of hydrogen bonding in the stabilization of the dihydrate structure.

Crystal Dehydration

The dehydration behaviour was studied by polarized light thermal microscopy at 0% RH and room temperature conditions, as well as at elevated temperatures. Microscopic observation of dihydrate crystals under crossed polarisers

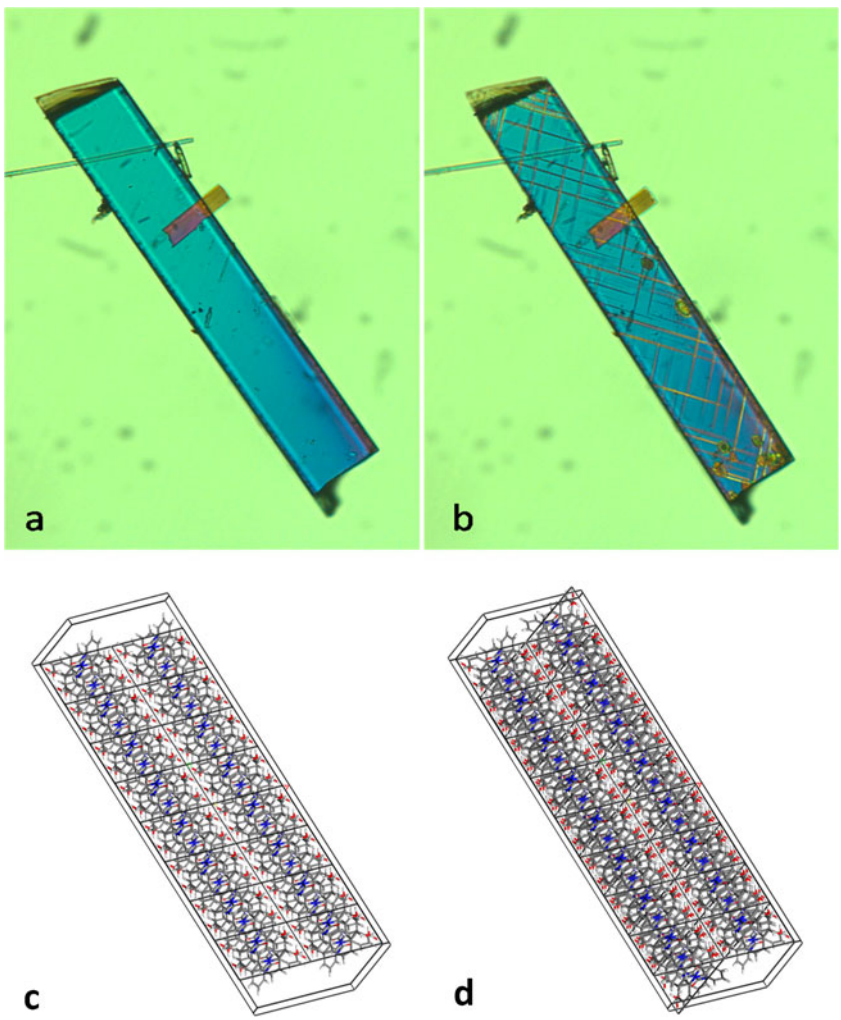

Fig. 3 Dihydrate crystals under partially crossed polarisers at 0% RH and ambient temperature, before (**a**) and after dehydration (**b**), showing the formation of a latticed texture on the (020) face, and projection of the crystal structure onto the (020) face (**c**,**d**).

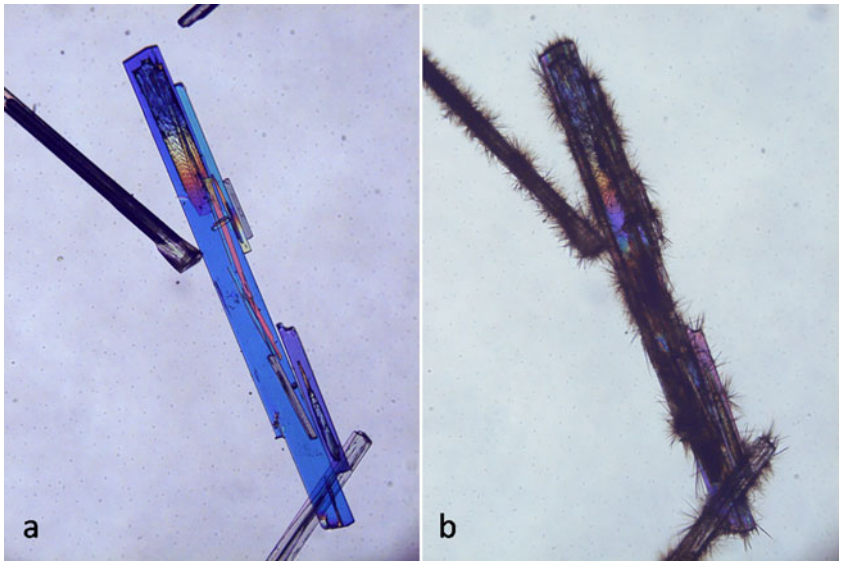

Fig. 4 Dihydrate crystals under partially crossed polarisers at 60°C, before and after dehydration, showing the formation of needle-shaped crystallites on the surfaces.

at 0% RH and ambient temperature revealed the formation of a latticed texture on the (020) face (Fig. 3) that is accompanied by progressive loss of birefringence, indicating amorphization. The latticed texture consists of parallel cracks that run in opposite directions on the (020) face, at an angle of 40.6± 1.2° to the elongation axis, crossing at 81.5±1.6°. The same texture appears when the crystals are heated below the glass transition point, typically near 50°C. When the crystals are immersed in silicone oil, additionally to the lattice texture, occasional cracking along the elongation axis and bubble formation are observed, suggesting release of crystal water.

Cracking and formation of surface texture while preserving the overall shape of the crystal (pseudomorphosis) is rather common in dehydrating crystals (38,39), and has been attributed to bulk shrinkage of the crystal, while quantitative models to predict the movement of the fracture front have been developed (40). However the highly ordered patterns observed in the case of carbamazepine are unusual, and have been attributed to the mechanism of dehydration (41). A projection of the crystal structure onto the (020) plane that can help elucidate the origins of cracking in the dehydrating crystals is

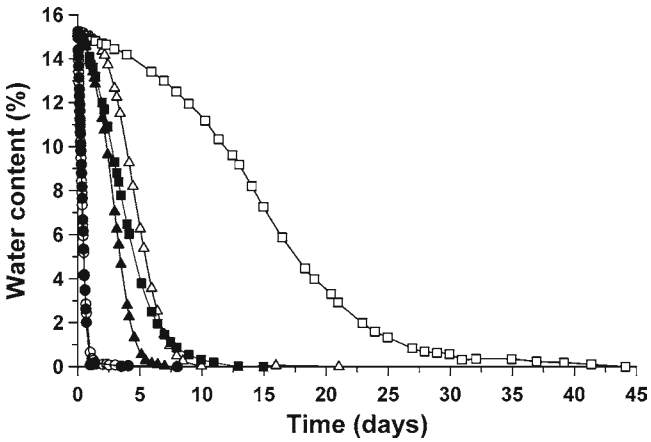

Fig. 5 Mass change *versus* time plots for the large (empty symbols) and small size fractions (full symbols) at 0% (●), 9% (▲) and 24% (■) RH.

Table IV Correlation Coefficients of the Kinetic Models Fitted to the Gravimetric Moisture Desorption Data Obtained at Different Relative Humidity Environments

Kinetic model	large size fraction		small size fraction	
	r	sd	r	sd
Nucleation models				
B1	0.9935	0.009	0.9923	0.006
A1	0.9937	0.007	0.9926	0.006
A2	0.9966	0.005	0.9957	0.003
A3	0.9980	0.001	0.9972	0.002
A4	0.9943	0.005	0.9933	0.006
P2	0.9781	0.009	0.9779	0.016
P3	0.9677	0.014	0.9668	0.022
P4	0.9613	0.016	0.9601	0.024
Geometric contraction models				
R2	0.9957	0.004	0.9940	0.005
R3	0.9919	0.006	0.9898	0.008
Diffusion models				
D1	0.9849	0.008	0.9800	0.010
D2	0.9704	0.011	0.9627	0.017
D3	0.9359	0.016	0.9280	0.026
D4	0.9607	0.012	0.9524	0.020
Reaction order models				
F0	0.9938	0.002	0.9941	0.006
F1	0.9756	0.012	0.9737	0.014
F2	0.8621	0.046	0.8713	0.040

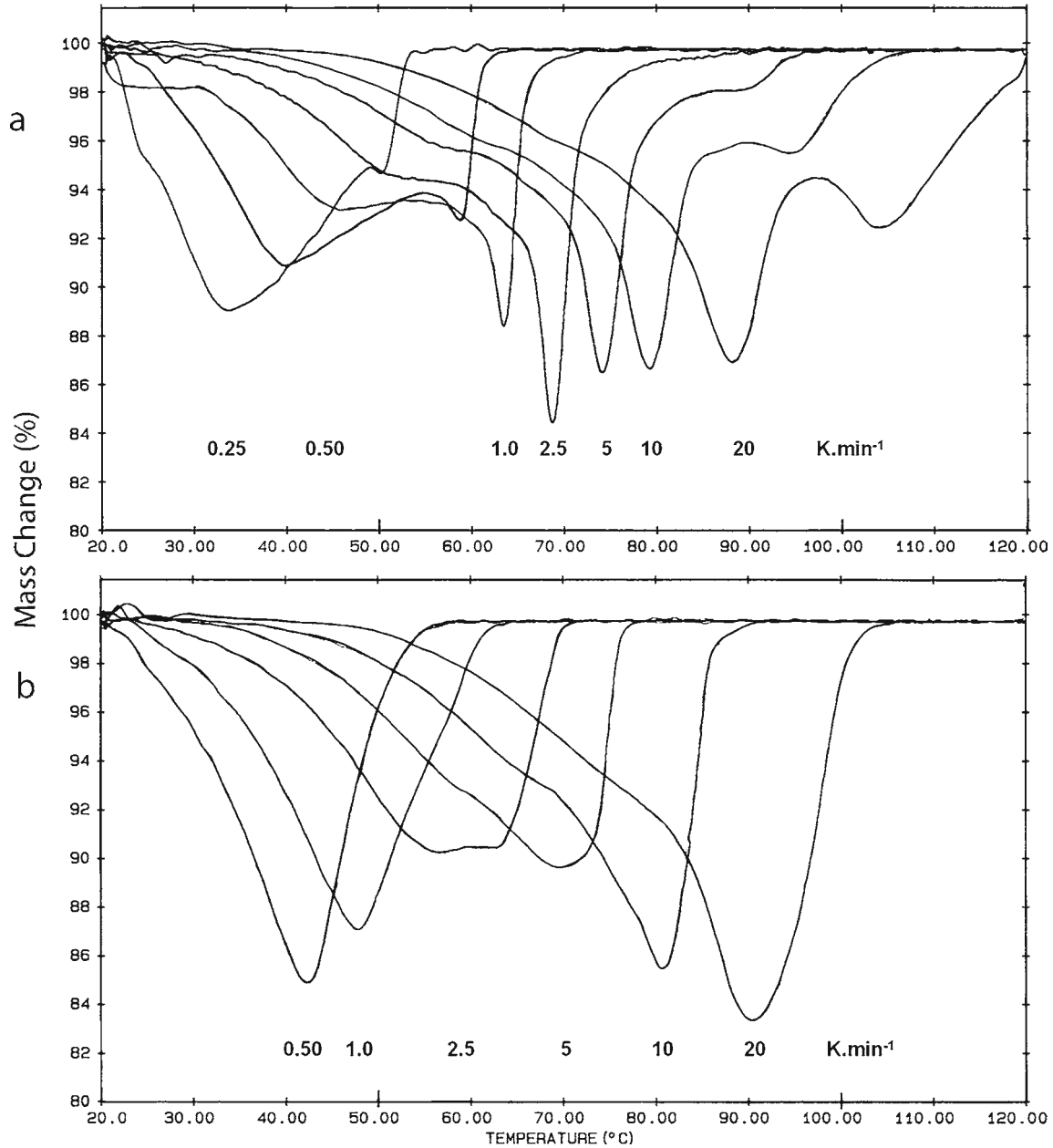

Fig. 6 Dynamic TGA curves (plots of mass change per unit time *vs* temperature) recorded at various heating rates for samples of large (**a**), and small (**b**) crystal size fraction.

shown in Fig. 3c,d. It is seen that the cracks along the elongation axis are perfectly aligned with the direction of the water channels running through the crystal lattice (Fig. 3c). Therefore it is probable that these cracks are the result of lattice shrinkage after emptying the space previously occupied by the water molecules. Molecular rearrangement by a concerted motion, rather than a collapse of the crystal lattice, should be responsible for the highly ordered latticed texture that appears following the departure of water molecules. Formation of cracks running in opposite direction can be explained considering the pseudo-merohedral micro-twinning by reflection in the mirror plane perpendicular to the α-axis (16), as shown in Fig. 3d.

When the crystals are heated at temperatures above the glass transition temperature of ~53°C, (42), nuclei of the anhydrous polymorph I start to form and the dehydration is complete by 75°C. Upon further heating, sublimation of needle-shaped and prismatic crystals takes place at 140°C, while needles of form I grow at the surfaces of the dehydrated crystals. Finally, at 176°C the prismatic sublimates melt (indicating that they belong to the anhydrous form III), followed by the melting of needle-shaped crystals of form I

Table V Correlation Coefficients of the Kinetic Models Fitted to the TGA Data Obtained Isothermally

Kinetic model	large size fraction				small size fraction			
	<50°C		>50°C		<50°C		>50°	
	r	sd	r	sd	r	sd	r	sd
Nucleation models								
B1	0.9266	0.015	0.9781	0.011	0.9747	0.011	0.9759	0.011
A1	0.9102	0.013	0.9750	0.013	0.9655	0.014	0.9682	0.017
A2	0.9250	0.011	0.9822	0.011	0.9746	0.012	0.9772	0.014
A3	0.9499	0.009	0.9911	0.006	0.9881	0.008	0.9898	0.009
A4	0.9687	0.007	0.9936	0.002	0.9957	0.004	0.9960	0.004
P2	0.8339	0.014	0.9362	0.029	0.9154	0.026	0.9180	0.033
P3	0.8094	0.015	0.9165	0.033	0.8971	0.029	0.8978	0.035
P4	0.7962	0.015	0.9052	0.035	0.8869	0.030	0.8864	0.035
Geometric contraction models								
R2	0.9521	0.008	0.9942	0.004	0.9884	0.008	0.9914	0.010
R3	0.9684	0.006	0.9948	0.002	0.9949	0.004	0.9962	0.005
Diffusion models								
D1	0.9563	0.011	0.9934	0.005	0.9868	0.006	0.9909	0.009
D2	0.9831	0.006	0.9876	0.011	0.9939	0.001	0.9944	0.004
D3	0.9990	0.001	0.9586	0.021	0.9842	0.008	0.9774	0.018
D4	0.9916	0.004	0.9804	0.014	0.9933	0.004	0.9915	0.009
Reaction order models								
F0	0.8919	0.013	0.9742	0.018	0.9548	0.019	0.9600	0.025
F1	0.9913	0.003	0.9844	0.009	0.9978	0.002	0.9944	0.007
F2	0.9664	0.015	0.8677	0.029	0.9221	0.012	0.8989	0.038

at 189–190°C. Dispersion in high melting point silicone oil hinders sublimation and decelerates the dehydration process but does not affect the resultant crystal form. Dehydration typically starts at 60°C with the simultaneous formation of needle-shaped crystallites on the surfaces (Fig. 4) and attains maximum rate at 90°C.

Table VI Kinetic Parameters Calculated According to the Arrhenious (Energy of Activation, E_a, and Pre-exponential Factor, log*A*) and Eyring Equation (Enthalpy, $\Delta H^{\neq}$, and Entropy, $\Delta S^{\neq}$, of the Activated Complex), Together with the Corresponding Correlation Coefficients, *r*, for the Models Giving the Best Fit Over the Specified Temperature Ranges for the Large and Small Crystal Size Fractions

	Large size fraction		Small size fraction	
	D3, <50°C	R2, >50°C	F1, <50°C	F1, >50°C
Arrhenious equation				
r	0.9959	0.9998	0.9954	0.9968
E_a	65.73	158.74	68.99	99.91
log*A*	8.31	23.60	10.38	15.27
Eyring equation				
r	0.9956	0.9999	0.9950	0.9966
$\Delta H^{\neq}$	63.11	155.95	66.36	97.12
$\Delta S^{\neq}$	−94.47	197.71	−54.96	38.12

Dehydration Kinetics

For the mechanistic interpretation of the dehydration process, the dehydration kinetics was modelled both at room temperature and different RH conditions by gravimetric moisture sorption and at different temperatures by isothermal TGA. Mass change *versus* time plots for the two size fractions used in this study are given in Fig. 5. It is seen that at 0% RH the crystals of both size fractions dehydrate fast and the reaction is complete within 24 h. As the RH increases, the effect of size fraction (and therefore, surface area) becomes more pronounced. At 9% RH, the large size fraction dehydrates completely in 10 days, while the small crystals require 5 days, and at 24% RH the large fraction dehydrate in 30 days *vs* 10 days for the small. This dependence of the dehydration kinetics on the crystal size outlines the significant effect of the surface to volume ratio on the mechanism of dehydration.

Kinetic analysis of the isotherms using various kinetic equations of Table I allowed the identification of the sigmoidal equations (JMAK and Prout-Tomkins) as the best

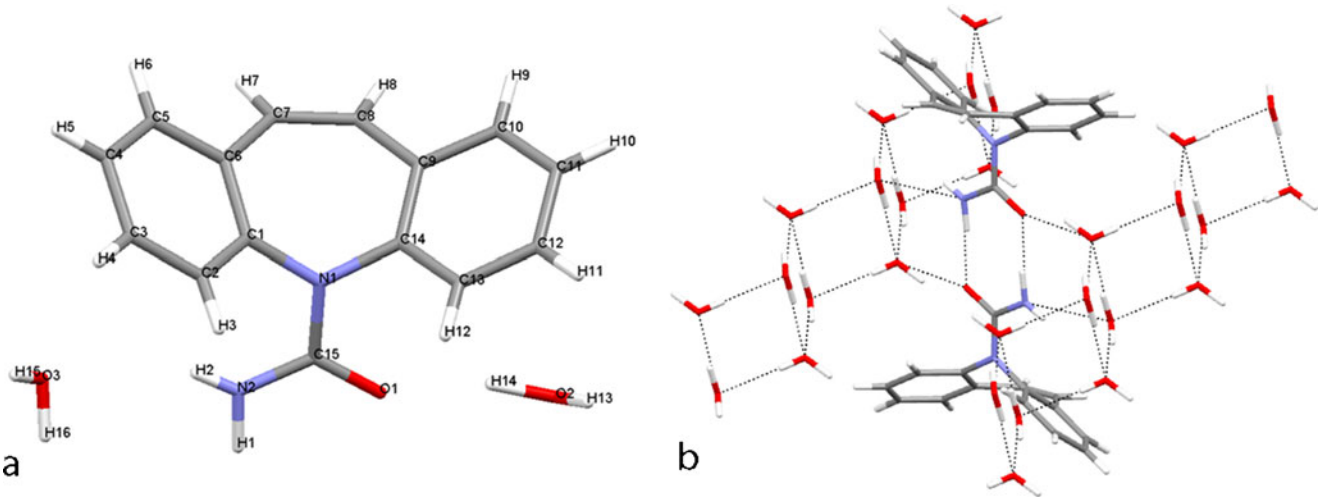

Fig. 7 View of the asymmetric unit of the dihydrate crystal unit cell, showing the numbering scheme (**a**), and the hydrogen bonding network (**b**).

fitting models (Table IV) with the A3 giving the best overall fit for both large and small size fractions at all three RH environments. The model implies three-dimensional nucleation of the anhydrous phase as the predominant mechanism of the dehydration. Microscopic observation of the dehydrated crystals revealed that the dehydrated product at 0% RH was amorphous, but at 9% and 24% it was crystalline, indicating that water acts as a plasticizer lowering the T_g of carbamazepine glass and increasing its tendency to crystallize. After 30 days of storage, the amorphous product obtained at 0% RH crystallized into form IV, while at 9% RH, form I was obtained, and at 24% RH the dehydration resulted in a mixture of forms I and III, identified by FTIR spectroscopy.

Dynamic TGA measurements at heating rates from 0.25 to 20 K/min (Fig. 6) showed that for the low heating rates, the dehydration begins at room temperature and is completed by 50°C, while it seems to be a biphasic process. This is more pronounced for the large crystal size fraction (Fig. 6a). As the heating rate increases, the dehydration starts at higher temperatures and proceeds faster. Regarding the isothermal TGA dehydration experiments, goodness of fit results of representative kinetic models (shown in Table I) to the isothermal TGA weight *vs* time data for the large and small size fraction of carbamazepine dihydrate, are listed in Table V, while parameters of the Arrhenious (energy of activation, E_a, pre-exponential factor, $logA$, and correlation coefficient, r) and Eyring (enthalpy, $\Delta H^{\neq}$, and entropy, $\Delta S^{\neq}$, of the activated complex, and correlation coefficient, r) equations for the large and small crystal size fraction calculated using the best fitting model, are listed in Table VI. It is remarkable that none of the tested kinetic models provided adequate fit over the whole temperature range, suggesting that the dehydration is a biphasic process and therefore the TGA data were split into two subsets. One subset consisted of data acquired in the 30–50°C temperature range (below the T_g) and the other covered the 50–70°C range (above the T_g). This improved the goodness of fit of the kinetic models significantly, indicating that the dehydration mechanism changes at the T_g. Specifically, for the large crystal size fraction, it is seen that at temperatures below the T_g, where dehydration results in amorphization, the best fitting model is the Jander diffusion equation (D3), which means that dehydration proceeds via three-dimensional diffusion of the water molecules. The relatively low value of the energy of activation (E_a=65.7 kJ/mol), which is close to the heat of evaporation of water, further supports a diffusion mechanism. However, at temperatures above the T_g, the reaction interface models (contracting cylinder, R2, and contracting sphere, R3) have the best fit, indicating that the dehydration rate is controlled by the interface formed between reactant (dihydrate) and product (crystalline, form I). This is confirmed by the increased value of the activation energy (E_a=158.7 kJ/mol). For the small crystal size fraction, the first order model describes best the dehydration reaction at all applied temperatures, however the activation energy increases significantly above the T_g (from 68.9 to 99.9 kJ/mol), reflecting the increased energy barrier that the water has to overcome when the dehydration product is crystalline.

Table VII Hydrogen Bond Geometry (D-H···A Distances and Angles, Where D Signifies the Donor and A the Acceptor Atom, Respectively) for the Optimized Crystal Structure by 3D Periodic DFT Calculations (Atom Numbering as in Fig. 7a)

D-H···A	Distance (Å)			Angle (°)
	D-H	H···A	D···A	D-H···A
N2-H2···O3	1.02	2.39	3.22	138.37
C15-O1···H14	0.99	1.89	2.84	161.99

From the Eyring equation parameters (Table VI) it is seen that for both crystal size fractions below the T_g the $\Delta H^{\neq}$ values are low (63.1 and 66.4 kJ/mol for the large and small crystal size fraction, respectively), corresponding to a fast reaction, however, the low $\Delta H^{\neq}$ values are compensated by the large negative values of $\Delta S^{\neq}$ (−94.5 and −54.6 J/K.mol for the large and small crystal size fraction, respectively), indicating that the reaction is unfavourable and that some degrees of freedom are frozen on the way to the transition state. Above the T_g the $\Delta H^{\neq}$ values increase reflecting the deceleration of the dehydration reaction (155.9 and 97.1 kJ/mol for the large and small crystal size fraction, respectively), while the $\Delta S^{\neq}$ becomes positive (197.7 and 38.1 J/K.mol for the large and small crystal size fraction, respectively), indicating that the reaction is favourable. The slower rate suggested by the increased $\Delta H^{\neq}$ values could be a result of the interface formed between the reactant (dihydrate) and product (form I).

Crystal Water Dynamics

In order to understand the dynamics of the dehydration process, the crystal structure of the dihydrate and in particular the hydrogen bonding patterns between water and carbamazepine molecules has to be considered. Figure 7 illustrates the asymmetric unit of the crystal (Fig. 7a), and the hydrogen bonding network formed by the water molecules (Fig. 7b), while hydrogen bond parameters based on the DFT-optimized geometry are listed in Table VII. It is seen that water molecules form two parallel infinite chains interconnected through hydrogen bonds. Additionally, the water molecules of each parallel chain form alternating hydrogen bonds to the amidic C=O and NH_2 groups of carbamazepine molecules. These hydrogen bonds differ in energy and the disruption of the hydrogen bonding network during dehydration should be a complex process, involving the reorientation of several chemical groups.

Insight into the course of this reaction and the temporal relationship of the submolecular movements taking place, can be gained by monitoring the changes of the FTIR absorption frequencies of the groups that are associated with the two crystallographically independent water molecules by hydrogen bonding. Figure 8 illustrates ATR-FTIR spectra of the dihydrate together with the most commonly occurring anhydrous forms I, III and IV, while Figs. 9 and 10 show synchronous and asynchronous correlation maps of the amide C=O (at 1670 cm^{-1}) and N-H stretching vibration (at 3432 cm^{-1} for the dihydrate, 3481 cm^{-1} for form I, and 3470 cm^{-1} for form IV), during dehydration below and above the glass transition temperature of carbamazepine, respectively.

At temperatures below 50°C (below the glass transition point), where formation of amorphous carbamazepine precedes nucleation and growth of form IV, the synchronous correlation map between the amide C=O and N-H stretching vibration (Fig. 9a) shows negative correlation, indicating that the two peaks change in opposite directions. The C=O peak increases, while the N-H peak decreases as the hydrogen bonds with the crystal water molecules break and the water is released to the environment. The positive sing of the correlation peaks between these two moieties in the asynchronous map (Fig. 9b) indicates that the C=O peak changes faster than the corresponding N-H peak. This means that the water associated with the amide C=O group departs faster than the water molecule attached to the amide N-H group. As proven by hot stage microscopy observations, its removal is accompanied by amorphization followed by the growth of

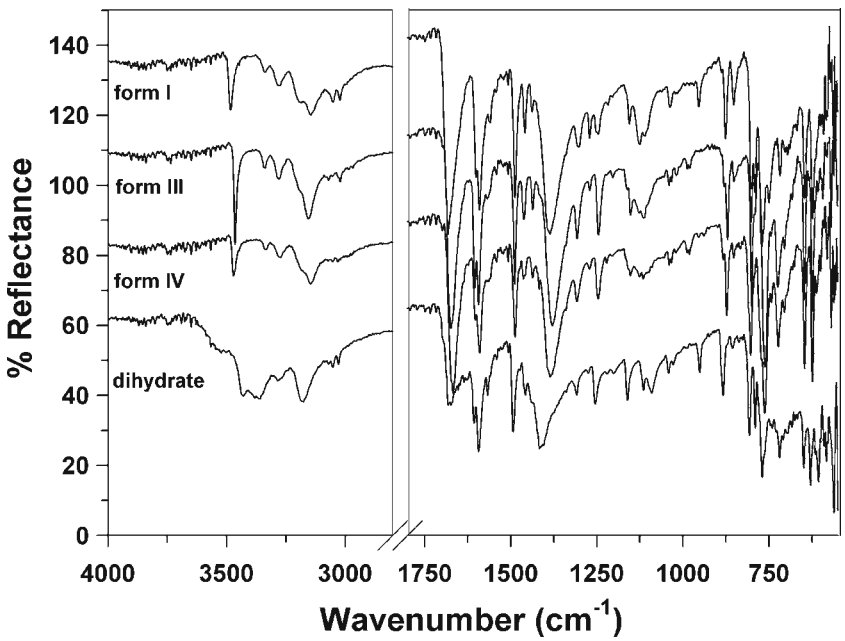

Fig. 8 ATR-FTIR spectra of pure forms I, III and IV, and the dihydrate.

form IV. Inspection of the correlation maps in the amide N-H region (Fig. 9c-d) reveals absence of correlation between the amide N-H of the dihydrate (3432 cm^{-1}) and form IV (3470 cm^{-1}). According to Noda's rules (33), when the synchronous correlation is zero, the temporal relationship between these two reorientations cannot be determined. This is probably because growth of form IV starts at a late stage of dehydration, after amorphization is almost complete, and proceeds by random nucleation.

At 60°C (above the glass transition point), the correlation maps shown in Fig. 10a–d, reveal that besides to the negative synchronous correlation between the amide C=O and N-H groups of the dihydrate, there is positive correlation between the C=O and N-H at 3481 cm^{-1}, that belongs to the growing form I, while the asynchronous correlation between the two moieties is zero. Correlation maps between the amide N-H groups of the dihydrate (3432 cm^{-1}) and form I (3481 cm^{-1}), additionally to the expected negative synchronous correlation, also exhibit a negative asynchronous correlation peak. According to Noda's rules, the absence of an asynchronous correlation peak between the dihydrate C= and the N-H peak of form I, and the same sign of the synchronous and asynchronous correlation peaks of the N-H group of these forms, indicates that the growth of form I initiates simultaneously

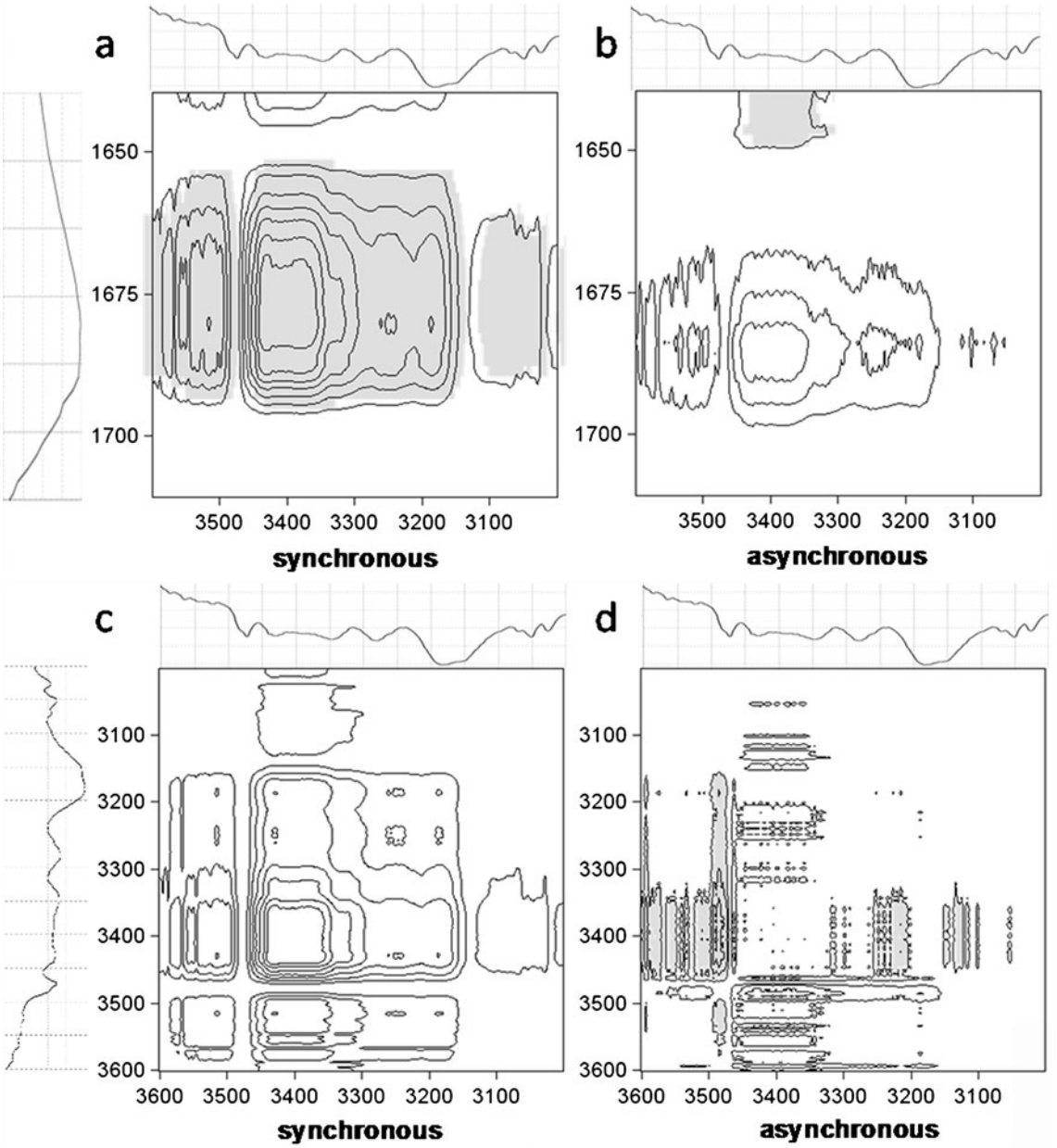

Fig. 9 Synchronous and asynchronous correlation maps between characteristic FTIR absorption bands obtained at 45 °C. Shaded areas indicate negative correlation.

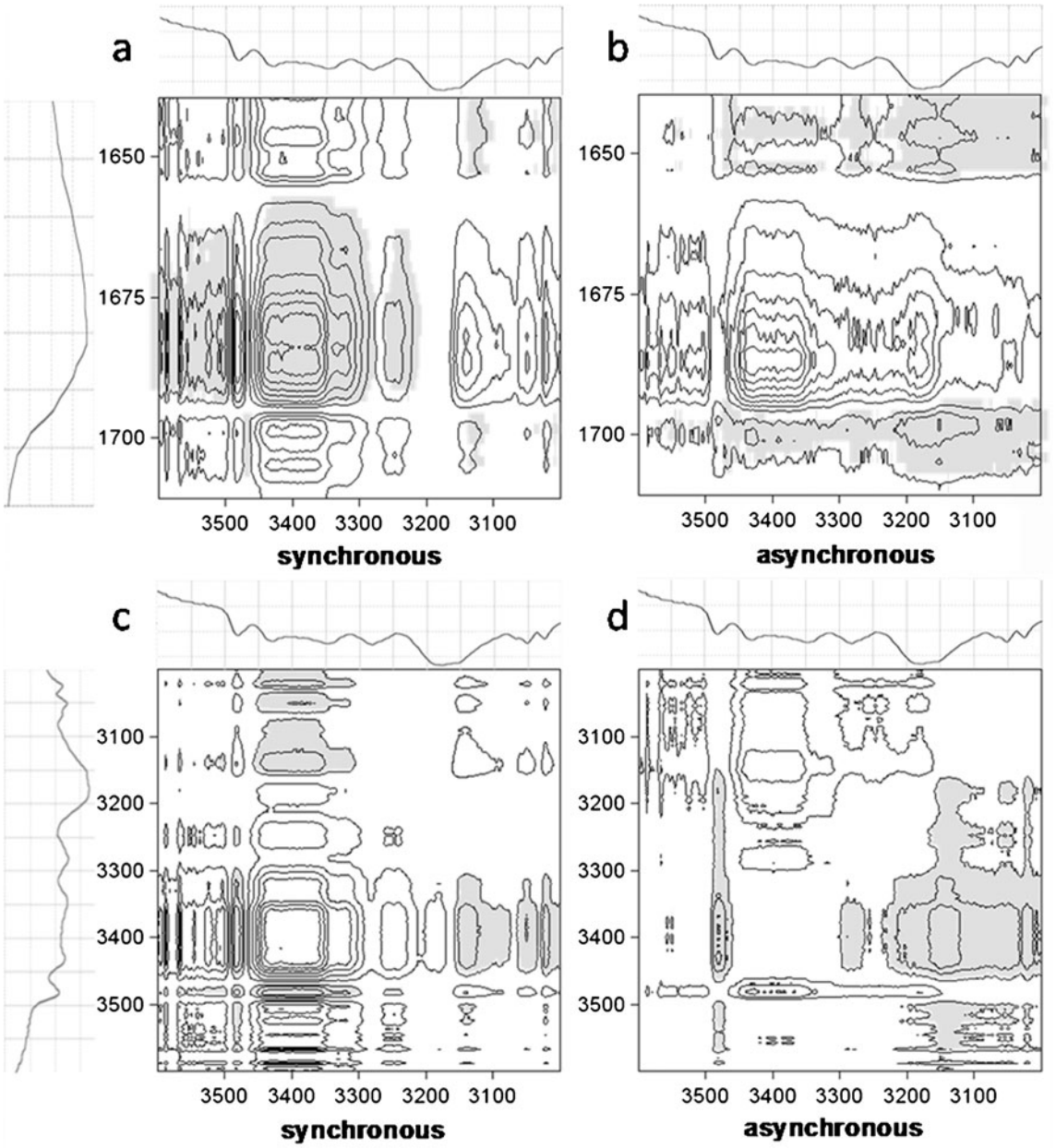

Fig. 10 Synchronous and asynchronous correlation maps between characteristic FTIR absorption bands obtained at 60 °C. Shaded areas indicate negative correlation.

with the departure of the crystal water attached to the C=O group, and proceeds at a faster rate than the departure of the crystal water attached to the N-H group, indicating that nucleation of form I is the rate controlling step of the reaction, in agreement with the kinetic modelling results.

Considering that the H···O distance of the hydrogen bond formed by the C=O group and the crystal water molecule is shorter than the one formed between the N-H group and the second water molecule (1.8 *vs* 2.6 Å in the optimized geometry), it is expected that this hydrogen bond should be stronger, and it is not clear why it breaks first. According to the classification of water environments in molecular hydrates (43), the water molecule attached to the carbonyl oxygen is classified as "environment 6" (H-bonded to two other water molecules and the CBZ carbonyl), while the water molecule attached to the amide N-H group is classified as "environment 5" (a single H-bond on the oxygen atom, and both hydrogens bonded to other water molecules). Environment "5" is statistically the most common environment, followed by "6", possibly reflecting the order of stability. In order to have a better insight into the hydrogen bonding between water and carbamazepine, the crystal orbital Hamilton population (COHP), obtained by periodic DFT calculations, was plotted for the 2p orbital of the oxygen and nitrogen atoms and the 1 s orbital of the hydrogen atom involved in the examined hydrogen bonds (Fig. 11). It is seen that there is negative overlap between the

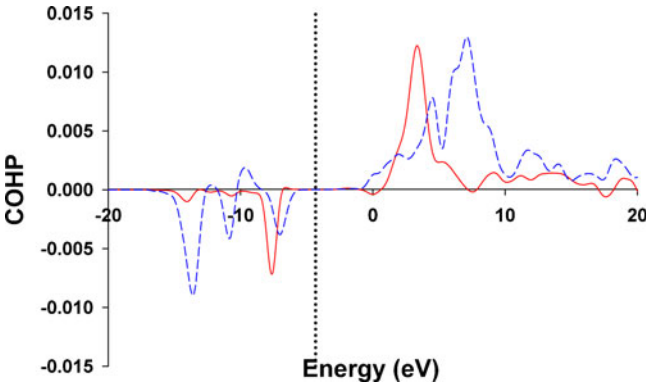

Fig. 11 Plots of crystal orbital Hamilton population (COHP) for the 2p orbital of the amide oxygen and nitrogen atoms and the 1 s orbital of the water hydrogen atoms involved in corresponding hydrogen bonds. The dotted line indicates the Fermi level.

amide hydrogen 1 s and the water oxygen 2p orbital Hamilton populations, as well as between the carbonyl oxygen 2p and the water hydrogen 1 s orbital Hamilton populations, indicating the formation of a hydrogen bond. Although in the case of the C=O···H hydrogen bond, the negative overlap is more extensive (as expected, due to the close contact between the two atoms), there is also a significant anti-bonding interaction indicated by the positive overlap (Fig. 11). Anti-bonding interactions are repulsive and destabilize a bond, and this should be the reason for the easier disruption of this hydrogen bond during the dehydration.

CONCLUSIONS

The dehydration of carbamazepine dihydrate consists of two overlapping processes strongly dependent on the environmental conditions, that occur at different rates and define the final product: a fast process comprising the removal of the less strongly bound water molecule attached to the amide C=O that leads to amorphization, and a slow process comprising the removal of the more strongly bound water molecule attached to the amide N-H group, followed by slow crystallization of form IV below the T_g or fast growth of form I above the T_g. The approach followed in this study is proven advantageous over the conventional reaction kinetics methodology, because it considers the structural features of the crystal lattice and energetic aspects of intermolecular interactions, additionally providing insight to the dynamics of crystal water. However it should be noted that the presented methodology is limited to hydrates of known crystal structure if we want a full interpretation of the spectral correlation maps, while another limitation is posed by the lack of widely available, reliable methods and software that allow the calculation of the electronic structure of organic solids, for which the importance of Van der Waals interactions cannot be ignored.

REFERENCES

1. Khankari R, Grant DJW. Pharmaceutical hydrates. Thermochim Acta. 1995;248:61–79.
2. Giron D, Goldbronn C, Mutz M, Pfeffer S, Piechon P, Schwab P. Solid state characterizations of pharmaceutical hydrates. J Thermal Anal Calorim. 2002;68:453–65.
3. Petit S, Coquerel G. Mechanism of several solid-solid transformations between dihydrated and anhydrous copper(II) 8-hydroxyquinolinates. Proposition for a unified model for the dehydration of molecular crystals. Chem Mater. 1996;8:2247–58.
4. Galwey AK. Structure and order in thermal dehydrations of crystalline solids. Thermochim Acta. 2000;355:181–238.
5. Jørgensen A, Strachan C, Pöllänen K, Koradia V, Tian F, Rantanen J. An insight into water of crystallization during processing using vibrational spectroscopy. J Pharm Sci. 2009;98:3903–32.
6. Beard M, Ghita O, McCabe J, Evans K. Monitoring dehydration kinetics using simultaneous thermal and spectral methods. J Raman Spectrosc. 2010;41:1283–8.
7. Agbada C, York P. Dehydration of theophylline monohydrate powder – effects of particle size and sample weight. Int J Pharm. 1994;106:33–40.
8. Sheth A, Zhou D, Muller F, Grant DJW. Dehydration kinetics of piroxicam monohydrate and relationship to lattice energy and structure. J Pharm Sci. 2004;93:3013–26.
9. Han J, Suryanarayanan R. Influence of environmental conditions on the kinetics and mechanism of dehydration of carbamazepine dihydrate. Pharm Dev Technol. 1998;3:587–96.
10. Yoneda S, Sugawara Y, Urabe H. Crystal water dynamics of guanosine dihydrate: analysis of atomic displacement parameters, time profile of hydrogen-bonding probability, and translocation of water by MD simulation. J Phys Chem B. 2005;109:1304–12.
11. Grzesiak A, Lang M, Kim K, Matzger A. Comparison of the four anhydrous polymorphs of carbamazepine and the crystal structure of form I. J Pharm Sci. 2003;92:2260–71.
12. Reck G, Dietz G. The order–disorder structure of carbamazepine dihydrate: 5 H-dibenz[b, f]azepine-5-carboxamide dihydrate, $C_{15}H_{12}N_2O.2H_2O$. Cryst Res Technol. 1986;21:1463–8.
13. Fleischman S, Kuduva S, McMahon J, Moulton B, Bailey Walsh R, Rodriguez-Hornedo N, Zaworotko M. Crystal engineering of the composition of pharmaceutical phases: multiple-component crystalline solids involving carbamazepine. Cryst Growth Des. 2003;3:909–19.
14. Meyer M, Straughn A, Jarvi E, Wood G, Pelsor F, Shah V. The bioinequivalence of carbamazepine tablets with a history of clinical failures. Pharm Res. 1992;9:1612–6.
15. Kobayashi Y, Ito S, Itai S, Yamamoto K. Physicochemical properties and bioavailability of carbamazepine polymorphs and dihydrate. Int J Pharm. 2000;193:137–46.
16. Harris R, Ghi P, Puschmann H, Apperley D, Griesser UJ, Hammond R, Ma C, Roberts K, Pearce G, Yates J, Pickard C. Structural studies of the polymorphs of carbamazepine, its dihydrate, and two solvates. Org Process Res Dev. 2005;9:902–10.
17. Gelbrich T, Hurtshouse M. Systematic investigation of the relationships between 25 crystal structures containing the carbamazepine molecule or a close analogue: a case study of the XPac method. Cryst Eng Comm. 2006;8:448–60.
18. Kogan A, Popov I, Uvarov V, Cohen S, Aserin A, Garti N. Crystallization of carbamazepine pseudopolymorphs from nonionic microemulsions. Langmuir. 2008;24:722–33.
19. Dugue J, Ceolin R, Rouland JC, Lepage F. Polymorphism of carbamazepine-solid state studies. Pham Acta Helv. 1991;66:307–10.
20. Griesser UJ. Untersuchungen zur Polymorphie und Pseudopolymorphie von Arzneistoffen de Pharmacopoea Europaea unter

besondered Berücksichtigung wasserhaltiger Kristallformen. Dissertation, University of Innsbruck. 1991.
21. Li Y, Han J, Zhang G, Grant D, Suryanarayanan R. *In situ* dehydration of carbamazepine dihydrate: a novel technique to prepare amorphous anhydrous carbamazepine. Pharm Devel Technol. 2000;5:257–66.
22. Surana R, Pyne A, Suryanarayanan R. Solid-vapor interactions: influence of environmental conditions on the dehydration of carbamazepine dihydrate. Pharm Sci Tech. 2003;4:1–10.
23. Murphy D, Rodríguez-Cintrón F, Langevin B, Kelly RC, Rodríguez-Hornedo N. Solution-mediated phase transformation of anhydrous to dihydrate carbamazepine and the effect of lattice disorder. Int J Pharm. 2002;246:121–34.
24. Kogermann K, Aaltonen J, Strachan C, Pöllänen K, Veski P, Heinämäki J, Yliruusi J, Rantanen J. Qualitative *in situ* analysis of multiple solid-state forms using spectroscopy and partial least squares discriminant modeling. J Pharm Sci. 2007;96:1802–20.
25. McMahon L, Timmins P, Williams A, York P. Characterization of dihydrates prepared from carbamazepine polymorphs. J Pharm Sci. 1996;85:1064–9.
26. Otsuka M, Ofusa T, Matsuda Y. Effect of environmental humidity on the transformation pathway of carbamazepine polymorphic modifications during grinding. Colloids Surf B Biointerfaces. 1999;13:163–273.
27. Fleming S, Rohl A. *GDIS*: a visualization program for molecular and periodic systems. Z Kristallogr. 2005;220:580–4.
28. Gale J, Rohl A. The General Utility Lattice Program (GULP). Molec Sim. 2003;29:291–341.
29. Mayo S, Olafson B, Goddard III W. DREIDING: a generic force field for molecular simulations. J Phys Chem. 1990;94:8897–909.
30. Jakalian A, Bush B, Jack D, Bayly C. Fast, efficient generation of high-quality atomic charges. AM1-BCC model: I. Method. J Comput Chem. 2000;21:132–46.
31. Jakalian A, Jack D, Bayly C. Fast, efficient generation of high-quality atomic charges. AM1-BCC model: II. Parametrization and validation. J Comput Chem. 2000;23:1623–41.
32. Eyring H. The activated complex in chemical reactions. J Chem Phys. 1935;3:107–15.
33. Noda I. Two-dimensional infrared (2D IR) spectroscopy: theory and applications. Appl Spectrosc. 1990;44:550–61.
34. Troullier N, Martins JL. Efficient pseudopotentials for plane-wave calculations. Phys Rev B. 1991;43:1993–2006.
35. Dion M, Rydberg H, Schröder E, Langreth D, Lundqvist B. Van der Waals density functional for general geometries. Phys Rev Lett. 2004;92:1–4.
36. Dronskowski R, Bloechl P. Crystal orbital Hamilton populations (COHP): energy-resolved visualization of chemical bonding in solids based on density-functional calculations. J Phys Chem. 1993;97:8617–24.
37. Soler JM, Artacho E, Gale J, García A, Junquera J, Ordejón P, Sánchez-Portal D. The SIESTA method for ab initio order-*N* materials simulation. J Phys Condens Matter. 2002;14:2745–79.
38. Griesser UJ. The importance of solvates. In: Hilfiker R, editor. Polymorphism in the pharmaceutical industry. Weinheim: Wiley-VCH; 2006. p. 224.
39. Brown M, Galwey AK, Guarini G. Structures and functions of reaction interfaces developed during solid-state dehydrations. J Thermal Anal. 1997;49:1135–46.
40. Chizhik S, Sidel'nikov A. Kinetics of solid state reactions with a positive feedback between the reaction and fracture: 1. A quantitative model for movement of the fracture front. Russ Chem Bull. 1998;47:604–9.
41. Khoo JY, Williams D, Heng J. Dehydration kinetics of pharmaceutical hydrate: effects of environmental conditions and crystal forms. Dry Technol. 2010;28:1164–9.
42. Patterson J, James M, Forster A, Lancaster R, Butler J, Rades T. The influence of thermal and mechanical preparative techniques on the amorphous state of four poorly soluble compounds. J Pharm Sci. 2005;94:1998–2012.
43. Gillon A, Feeder N, Davey R, Storey R. Hydration in molecular crystals – a Cambridge Structural Database analysis. Cryst Growth Des. 2003;3:663–73.